Architecture of the Complex Formed by Large and Small Terminase Subunits from Bacteriophage P22

Reginald McNulty[1†], Ravi Kumar Lokareddy[2,†], Ankoor Roy[2], Yang Yang[3], Gabriel C. Lander[1], Albert J.R. Heck[3], John E. Johnson[1] and Gino Cingolani[2]

1 - Department of Integrative Structural and Computational Biology, *The Scripps Research Institute, La Jolla, CA 92037, USA*
2 - Department of Biochemistry and Molecular Biology, *Thomas Jefferson University, 233 South 10th Street Philadelphia, PA 19107, USA*
3 - Biomolecular Mass Spectrometry and Proteomics, *Bijvoet Centre for Biomolecular Research and Utrecht Institute for Pharmaceutical Sciences, University of Utrecht, Netherlands Proteomics Center, Padualaan 8, 3584 CH Utrecht, The Netherlands*

Correspondence to Reginald McNulty and Gino Cingolani: *rmcnulty@scripps.edu; gino.cingolani@jefferson.edu*
http://dx.doi.org/10.1016/j.jmb.2015.08.013
Edited by M. F. Summers

Abstract

Packaging of viral genomes inside empty procapsids is driven by a powerful ATP-hydrolyzing motor, formed in many double-stranded DNA viruses by a complex of a small terminase (S-terminase) subunit and a large terminase (L-terminase) subunit, transiently docked at the portal vertex during genome packaging. Despite recent progress in elucidating the structure of individual terminase subunits and their domains, little is known about the architecture of an assembled terminase complex. Here, we describe a bacterial co-expression system that yields milligram quantities of the S-terminase:L-terminase complex of the *Salmonella* phage P22. *In vivo* assembled terminase complex was affinity-purified and stabilized by addition of non-hydrolyzable ATP, which binds specifically to the ATPase domain of L-terminase. Mapping studies revealed that the N-terminus of L-terminase ATPase domain (residues 1–58) contains a minimal S-terminase binding domain sufficient for stoichiometric association with residues 140–162 of S-terminase, the L-terminase binding domain. Hydrodynamic analysis by analytical ultracentrifugation sedimentation velocity and native mass spectrometry revealed that the purified terminase complex consists predominantly of one copy of the nonameric S-terminase bound to two equivalents of L-terminase (1S-terminase:2L-terminase). Direct visualization of this molecular assembly in negative-stained micrographs yielded a three-dimensional asymmetric reconstruction that resembles a “nutcracker” with two L-terminase protomers projecting from the C-termini of an S-terminase ring. This is the first direct visualization of a purified viral terminase complex analyzed in the absence of DNA and procapsid.

Introduction

Viral genome packaging is a complex, non-spontaneous reaction, catalyzed in many double-stranded DNA (dsDNA) viruses by a powerful genome-packaging motor [1–3]. This motor consists of a portal protein, which occupies one of the vertices of the icosahedral procapsid, and a terminase complex that converts ATP hydrolysis into linear translation of dsDNA. In most tailed phages, the terminase complex is formed by two subunits known as small terminase (referred to as S-terminase) and large terminase (referred to as L-terminase), whereas herpesviruses also have a third subunit of unknown function and structure [4]. The ATPase activity necessary to power genome packaging resides in the L-terminase subunit, which binds directly to the portal protein [5]. In contrast, the S-terminase subunit binds packaging initiation sites on the dsDNA (referred to as *pac* in P22 [6]) to prepare for genome packaging [7] and regulates the ATPase activity of L-terminase [8,9]. These functions are likely to be very important *in vivo* to sustain the enormous rate of genome packaging, which can be as high as ~2000 bp/s [10].

We previously characterized the L-terminase (499 amino acids, 57.6 kDa [11]) and S-terminase (162 amino acids, 18.6 kDa [7]) subunits of the bacteriophage P22 [12] (Fig. 1a), a prototypical

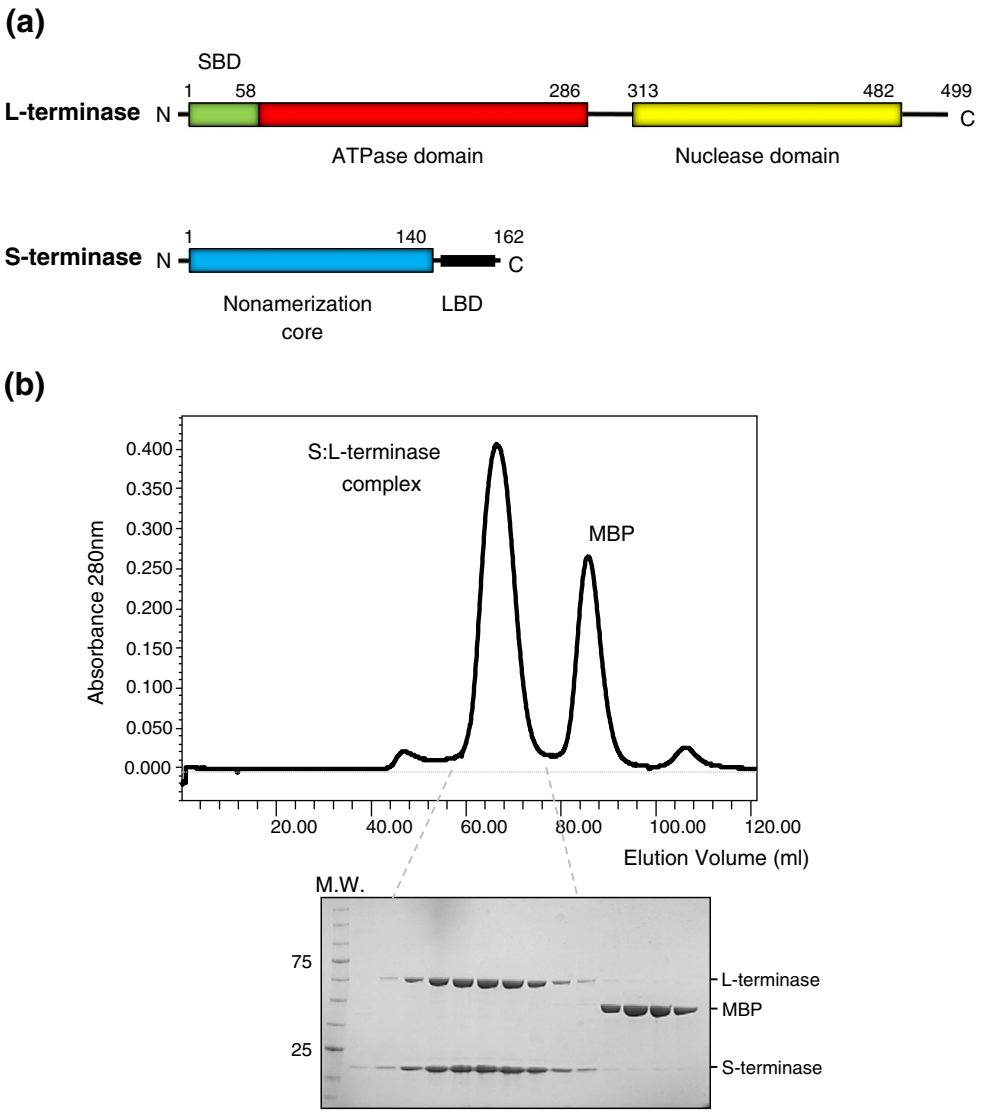

Fig. 1. Co-expression and purification of P22 S-terminase:L-terminase complex. (a) Domain organization of P22 S-terminase and L-terminase subunits. (b) Chromatogram of the S-terminase:L-terminase complex purified in the presence of mild detergent, magnesium chloride and glycerol. The S-terminase:L-terminase complex was separated on a Superdex 200 gel-filtration column after o/n digestion with PreScission Protease. Fractions corresponding to the eluted peaks were analyzed by SDS-PAGE (bottom gel) revealing pure S-terminase and L-terminase subunits and free MBP.

member of the *Podoviridae* family of short tailed bacteriophages. In this phage, S-terminase assembles in solution and in crystals as a hollow nonamer [13–15], similar to the S-terminase of the *Siphoviridae* SPP1-like phage Sf6 [16]. This oligomer is surprisingly different from the octameric S-terminase of phage Sf6 [17], also a *Podoviridae*, and the distant *Myoviridae* T4-like 44RR, which was determined crystallographically as a mixture of *undecamer* and dodecamers [18]. The way S-terminases bind to DNA varies in different viruses. In P22, all DNA-binding determinants are confined in a C-terminal basic moiety comprising residues 140–162, which also overlaps with the L-terminase binding domain (LBD) [13] (Fig. 1a). In contrast, in phage λ S-terminase (gpNu1) [19] and possibly in Sf6 [20] and T4 [18], DNA binding is thought to occur via an N-terminal winged helix–turn–helix motif. Unlike S-terminases that are highly divergent in sequence, structure and possibly mechanisms of DNA binding [21], all known L-terminase subunits have an N-terminal ATPase domain [22,23] that contains ATP-binding Walker A and B motifs, flexibly linked to a C-terminal RNase H-fold nuclease [24,25] also conserved in *Herpesviridae* [26,27].

DNA packaging in P22 proceeds by a “headful packing” mechanism, a packaging strategy where the length of the DNA encapsulated inside the

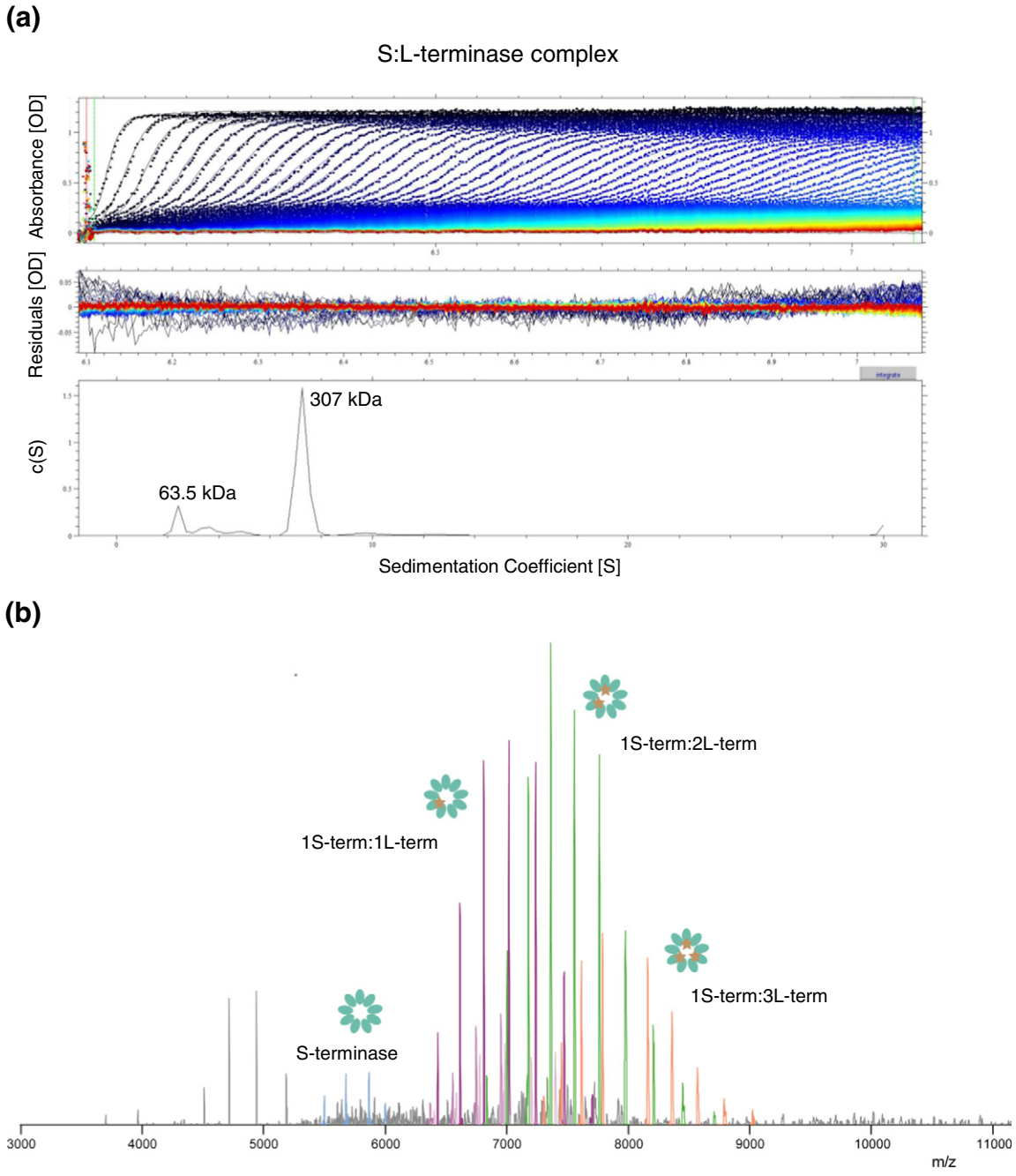

Fig. 2. Biophysical analysis of the purified S-terminase:L-terminase complex. (a) Sedimentation velocity profiles of the S-terminase:L-terminase complex measured in 20 mM Tris–Cl (pH 8.0), 150 mM NaCl, 3 mM DTT, 5% glycerol and 1 mM $MgCl_2$ at 10 °C. Top panel: raw absorbance at 280 nm plotted as a function of the radial position. Data at intervals of 20 min are shown as dots for sedimentation at 35,000 rpm. Middle panel: the residuals between fitted curve and raw data. Bottom panel: the fitted distribution of the apparent sedimentation coefficient (s^*) calculated for S-terminase:L-terminase is 7.2S (~85% sample) and 2.7S (<15% sample) corresponding to an estimated molecular mass of ~307 kDa and ~63.5 kDa, respectively. (b) Native MS analysis of the S-terminase:L-terminase complex. The following masses are observed: 1S-terminase:1L-terminase, 231.465 ± 0.002 kDa (purple peaks); 1S-terminase:2L-terminase, 286.989 ± 0.012 kDa (green peaks); 1S-terminase:3L-terminase, 342.514 ± 0.008 kDa (orange peaks); nonamer of S-terminase, 175.955 ± 0.002 kDa (magenta peaks).

procapsid is determined by the interior volume of the mature phage particle [28,29]. The exact molecular mechanisms by which S-terminase and L-terminase subunits orchestrate headful packaging are poorly understood. It was reported that P22 S-terminase and L-terminase form a complex that can be purified

from infected cells [30], but the stoichiometry of this terminase complex is unknown. Genetic evidence has shown that the DNA-recognition subunit, S-terminase, binds to packaging initiation sites (*pac*) [31] in the P22 genome and positions viral dsDNA for the packaging L-terminase subunit, which uses ATP hydrolysis to translocate a single genome copy into an empty procapsid. The substrate for DNA packaging in P22 is a repeating polymer containing up to 10 copies of phage genome, known as concatemer [32]. The L-terminase is thought to oligomerize at the portal vertex, as observed in T4 [22] and T7 [33], in order to facilitate packaging into empty P22 procapsid. The nuclease domain of L-terminase cleaves concatemeric dsDNA at two stages of the packaging reaction. At the beginning of packaging, the terminase makes sequence-specific cleavages in the *pac* region (referred to as "series initiation cleavage") to generate a DNA end and initiate a packaging series. The DNA end is then inserted into the procapsid unidirectionally from the initiation cleavage point in an ATP-dependent process catalyzed by the ATPase domain of L-terminase. Upon insertion typically between 102% and 110% of the genome length [34], the headful nuclease of L-terminase cleaves the DNA, releasing the concatemer from the newly filled particle and resulting in dissociation of the terminase complex from the capsid. This enables binding of the tail proteins gp4 [35–39], gp10 [40] and gp26 [40–42] that seal the portal protein and stabilize the genome inside the capsid, followed by the attachment of six copies of the tailspike gp9 [43]. Subsequent packaging events follow sequentially in a processive fashion, and each round of infection results in about 2% of newly replicated particles that carry host DNA instead of the viral chromosome [44].

Despite a growing number of structures of isolated S-terminase and L-terminase subunits, a complete view of a terminase complex is lacking. In this work, we purified the S-terminase:L-terminase complex of bacteriophage P22 and provide a structural characterization of its architecture by identifying biochemical interactions and employing hybrid structural methods.

Results

Purification of a homogeneous complex of P22 S-terminase and L-terminase subunits

L-terminases are intrinsically unstable enzymes, notoriously difficult to purify and prone to aggregation [22,30,33,45,46]. Previous attempts to reconstitute the S-terminase:L-terminase complex of bacteriophage P22 from purified nonameric S-terminase and monomeric L-terminase yielded a heterogeneous mixture [13]. As an alternative approach, we formed the terminase complex *in vivo* by co-expressing a plasmid encoding maltose binding protein (MBP)-tagged S-terminase and untagged L-terminase in bacteria (Fig. 1b), followed by purification of the S-terminase:L-terminase complex on amylose beads. The bead-immobilized complex was then incubated with 1 mM 5′-adenylyl-β,γ-imidodiphosphate (AMP-PNP) to stabilize the ATPase domain of L-terminase [30] and MBP cleaved off using PreScission Protease. We found that including traces of the non-ionic detergent *n*-dodecyl-β-D-maltoside (DDM) during cell lysis, in addition to magnesium chloride and 5% glycerol during purification greatly, reduced the tendency of terminase subunits to aggregate. The purified S-terminase:L-terminase complex migrated on a size-exclusion chromatography column as a monodisperse species with estimated molecular mass of ~300 kDa and was >90% pure by SDS-PAGE (Fig. 1b). Unlike individual terminase subunits that are highly susceptible to proteolysis [25], the complex remained stably assembled for days to weeks.

Solution biophysical analysis

To investigate the oligomeric state of the purified S-terminase:L-terminase complex, we subjected this species to analytical ultracentrifugation (AUC) sedimentation velocity analysis. Figure 2a shows a typical sedimentation profile of P22 terminase complex obtained in 150 mM sodium chloride, at 10 °C. In a range of concentration between 1 and 10 μM, the complex migrated as a largely homogeneous species characterized by one major component with an apparent sedimentation coefficient (s^*) of 7.2S (absolute sedimentation coefficient, S20,w = 9.6S). Conversion of this parameter into molecular mass revealed a molecular mass of ~307 ± 0.5 kDa possibly corresponding to a nonamer of S-terminase (~176 kDa) bound to two copies of L-terminase:AMP-PNP [~176 kDa + 2 × (55.9 + 0.5) = 288.8 kDa] or three copies of L-terminase:AMP-PNP [~176 kDa + 3 × (55.9 + 0.5) = 344.3 kDa]. Furthermore, the frictional ratio estimated based on sedimentation data was f/f_o ~ 1.7, suggestive of an elongated molecular assembly. A smaller species (<15% of the total sample) was also observed with a sedimentation coefficient consistent with free L-terminase, possibly resulting from complex dissociation during centrifugation.

The same purified S-terminase:L-terminase complex was also subjected to native mass spectrometry (MS) analysis. In agreement with AUC, we observed charge distributions corresponding to the mass of a single S-terminase:L-terminase complex. No larger aggregated species were observed. The spectrum at m/z 6500–9000 in Fig. 2b originates from one nonamer of the S-terminase bound to different numbers of copies of L-terminase. Up to three

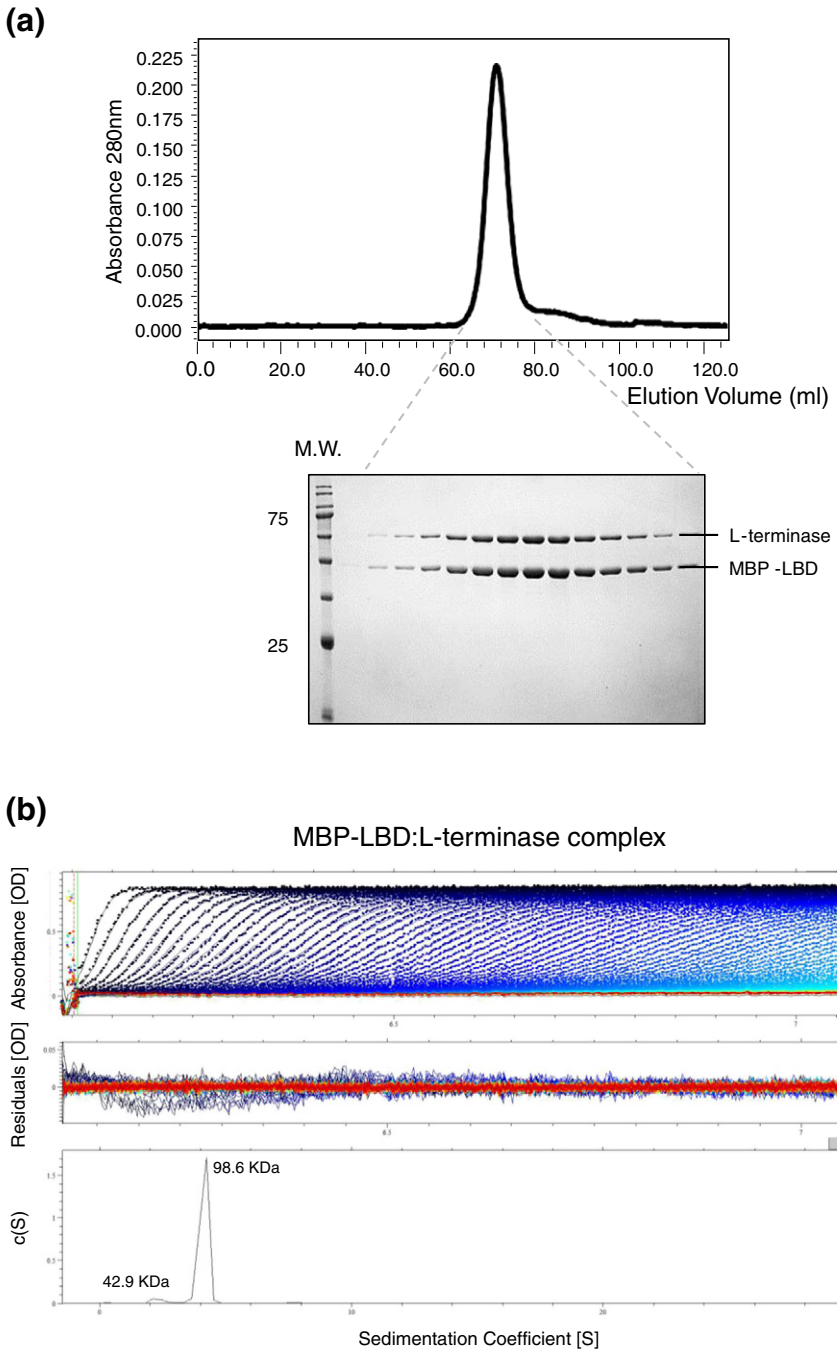

Fig. 3. Stoichiometric binding of L-terminase to the LBD. (a) Chromatogram of the purified MBP-LBD:L-terminase complex eluted with 10 mM maltose from amylose beads and separated on a Superdex 200 gel-filtration column. Fractions corresponding to the eluted peak were analyzed by SDS-PAGE (bottom gel) revealing a 1:1 stoichiometry of association between L-terminase and MBP-LBD. (b) Sedimentation velocity profiles of the MBP-LBD:L-terminase complex measured in 20 mM Tris–Cl (pH 8.0), 150 mM NaCl, 3 mM DTT, 5% glycerol and 1 mM $MgCl_2$ at 10 °C. Top panel: raw absorbance at 280 nm plotted as a function of the radial position. Data at intervals of 20 min are shown as dots for sedimentation at 40,000 rpm. Middle panel: the residuals between fitted curve and raw data. Bottom panel: the fitted distribution of the apparent sedimentation coefficient (**s***) calculated for S-terminase:L-terminase is 4.2S (~90% sample) and 2.7S (<10% sample) corresponding to an estimated molecular mass of ~98.6 kDa and ~42.9 kDa, respectively.

copies of L-terminase were confidently assigned binding to one S-terminase nonamer, based on accurate mass measurement made possibly by using the Orbitrap EMR platform [47]. Nonameric S-terminase and free L-terminase were also observed in the MS, at low abundance (<20%), possibly due to

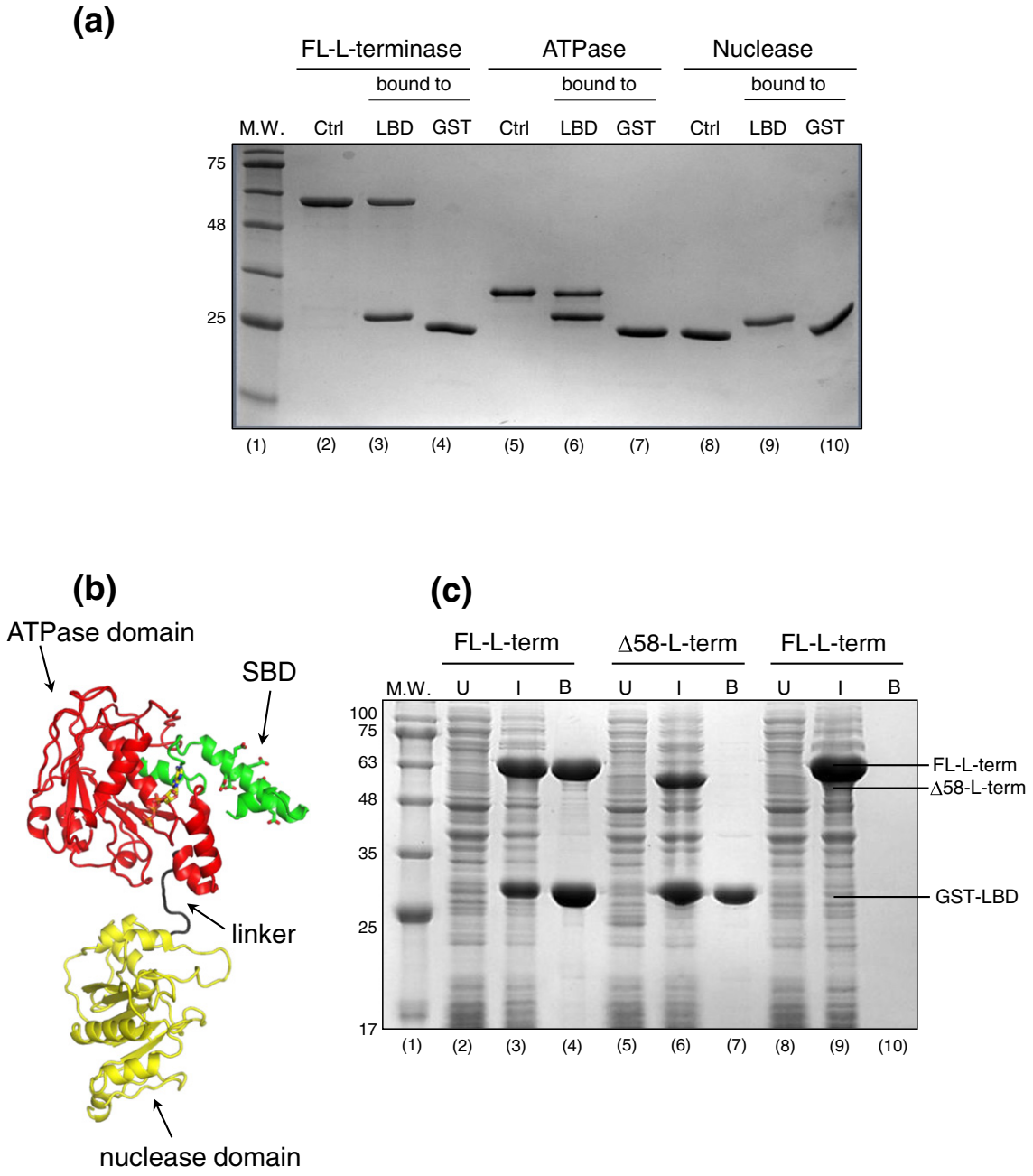

Fig. 4. The N-terminus of L-terminase ATPase domain binds specifically to the LBD. (a) Pull-down assay on glutathione beads coupled to GST-LBD reveals that L-terminase ATPase domain is sufficient for binding to S-terminase. (b) Ribbon diagram of a homology model of P22 L-terminase (generated using i-TASSER [67]) with SBD, ATPase and nuclease domains colored green, red and yellow, respectively. (c) Co-expression of FL-L-terminase and Δ58-L-terminase with GST-LBD in bacteria followed by pull-down on glutathione beads and SDS-PAGE analysis reveals that the SBD is essential for association with the LBD.

in-source dissociation during electrospray ionization. Thus, the predominant S-terminase:L-terminase complex assembled *in vivo* and purified *in vitro* consists of a nonameric S-terminase ring bound to two to three copies of L-terminase.

Stoichiometric binding of L-terminase to S-terminase LBD

The substoichiometric presence of L-terminase in the terminase complex and the small size of

S-terminase LBD (~22 residues) [13] prompted us to investigate if each L-terminase associates with multiple LBDs in the context of an assembled terminase complex. To address this question, we co-expressed in bacteria untagged L-terminase with MBP-tagged LBD (MBP-LBD) and purified milligram quantity of the complex using amylose beads. By size-exclusion chromatography, the MBP-LBD:L-terminase complex migrated as a homogeneous species of ~100 kDa (Fig. 3a), consistent with a heterodimer of the two proteins in 1:1 stoichiometry. A more accurate quantification was obtained by AUC sedimentation velocity, which gave an apparent sedimentation coefficient (s^*) for the complex of 4.2S (absolute sedimentation coefficient, S20,w = 4.4S) (Fig. 3b), corresponding to a mass of 98.6 kDa, unambiguously consistent with one copy of L-terminase:AMP-PNP bound to one copy of MBP-LBD (expected molecular mass of ~98.4 kDa). AUC studies also revealed that the MBP-LBD remains monomeric in solution at all concentrations tested (data not shown). Thus, each copy of L-terminase in the S-terminase:L-terminase complex is likely to associate with only one LBD.

Biochemical mapping of domains involved in terminase subunits association

We used an on-bead assay to determine the domain of L-terminase that associates with S-terminase. GST (*g*lutathione *S*-*t*ransferase)-tagged LBD (GST-LBD) was immobilized on glutathione beads and used to pull down either the full-length L-terminase (FL-L-terminase) or individually purified ATPase or nuclease domains. The ATPase domain alone associated specifically with GST-LBD with comparable avidity as the FL-L-terminase (Fig. 4a, lanes 6 and 3), but it failed to bind to glutathione beads not coupled to LBD (Fig. 4a, lane 7), suggesting that all binding determinants in L-terminase necessary for S-terminase assembly are confined in the N-terminal ATPase domain. In contrast, no binding was observed between L-terminase nuclease domain and GST-LBD (Fig. 4a, lane 9), ruling out the involvement of this domain in terminase subunit assembly.

To further map the region of L-terminase ATPase domain involved in LBD, we made the striking observation that P22 L-terminase contains an N-terminal extension of ~58 amino acids not found in closely related P22-like phages such as Sf6 [17] but conserved in phages whose S-terminase also bears a C-terminal LBD [48]. A homology model of P22 L-terminase revealed that this N-terminal extension folds into a helix–loop–helix, positioned near the ATP binding pocket, whereby the central helix is highly acidic and has propensity to form coiled-coil structures (Fig. 4b). Intrigued by the idea that this moiety in L-terminase represents a dedicated platform for binding to the highly basic S-terminase LBD, we generated a deletion construct of L-terminase lacking residues 1–58 (Δ58-L-terminase) and co-expressed it in bacteria with GST-LBD (Fig. 4c, lane 7). Unlike a positive control of FL-L-terminase (Fig. 4c, lane 4), we found no specific interaction of Δ58-L-terminase with LBD, comparable to a negative control where a lysate expressing FL-L-terminase was passed on uncoupled GST beads (Fig. 4c, lane 10). Thus, S-terminase LBD associates with an N-terminal acidic extension of L-terminase ATPase domain that we will refer to as S-terminase binding domain (SBD) (Fig. 4b).

Visualization of the S:L-terminase complex by transmission electron microscopy

We used single-particle transmission electron microscopy to analyze the S-terminase:L-terminase complex in negative stain (Fig. S1). From a data set consisting of 44 images containing 6562 particles, analysis of the 2D (*2*-*d*imensional) class averages via Iterative Stable Alignment and Clustering (ISAC) revealed several orientations of the S-terminase:L-terminase complex (Fig. 5a). Although some heterogeneity was observed, many class averages resemble different views of one S-terminase nonamer bound to two L-terminase molecules. A total of 2062 particles were identified as belonging to the 1S-terminase:2L-terminase species using 3D (*3*-*d*imensional) classification analysis with Regularized Likelihood Optimization (RELION). To obtain an asymmetric 3D reconstruction, we used the crystal structure of the S-terminase nonamer low-pass filtered to 60 Å as an initial model (Fig. S2a). In addition to low-pass filtering, this model was unbiased in that it lacked density corresponding to L-terminase and comprised less than a third of the mass of the complex. On the other hand, the S-terminase nanomer was clearly visible by eye in many of the individual complexes making it an excellent initial model. Because of heterogeneity seen in 2D class averages, three classes were used during RELION 3D classification and refinement to separate poor and broken complexes from well-aligned particles. Two classes produced non-interpretable density, while a third showed two "new" elongated densities approximately 100 Å long, not included in the starting model, and presumed to correspond to two L-terminase molecules, beneath the S-terminase ring (Fig. 5b). The L-terminase molecules were oriented with their ATPase domains adjacent to the S-terminase since biochemical analysis described above confirmed that mode of interaction. Overall, the S-terminase:L-terminase complex resembles a "nutcracker", with two parallel L-terminase molecules positioned just below the mushroom-shaped S-terminase. The complex is approximately 100 Å wide and 150 Å long and presents a central lumen emanating from the S-terminase nonamer, which is readily visible in the reconstruction. The resolution of this reconstruction was estimated to be 30 Å using the FSC = 0.143

criterion (Fig. S2b) [49]. To validate this reconstruction, we matched the 2D class averages produced by ISAC analysis to corresponding 2D projections of the model obtained by RELION 3D classification and refinement and we show them at corresponding angles in Fig. 5c. This analysis revealed a striking

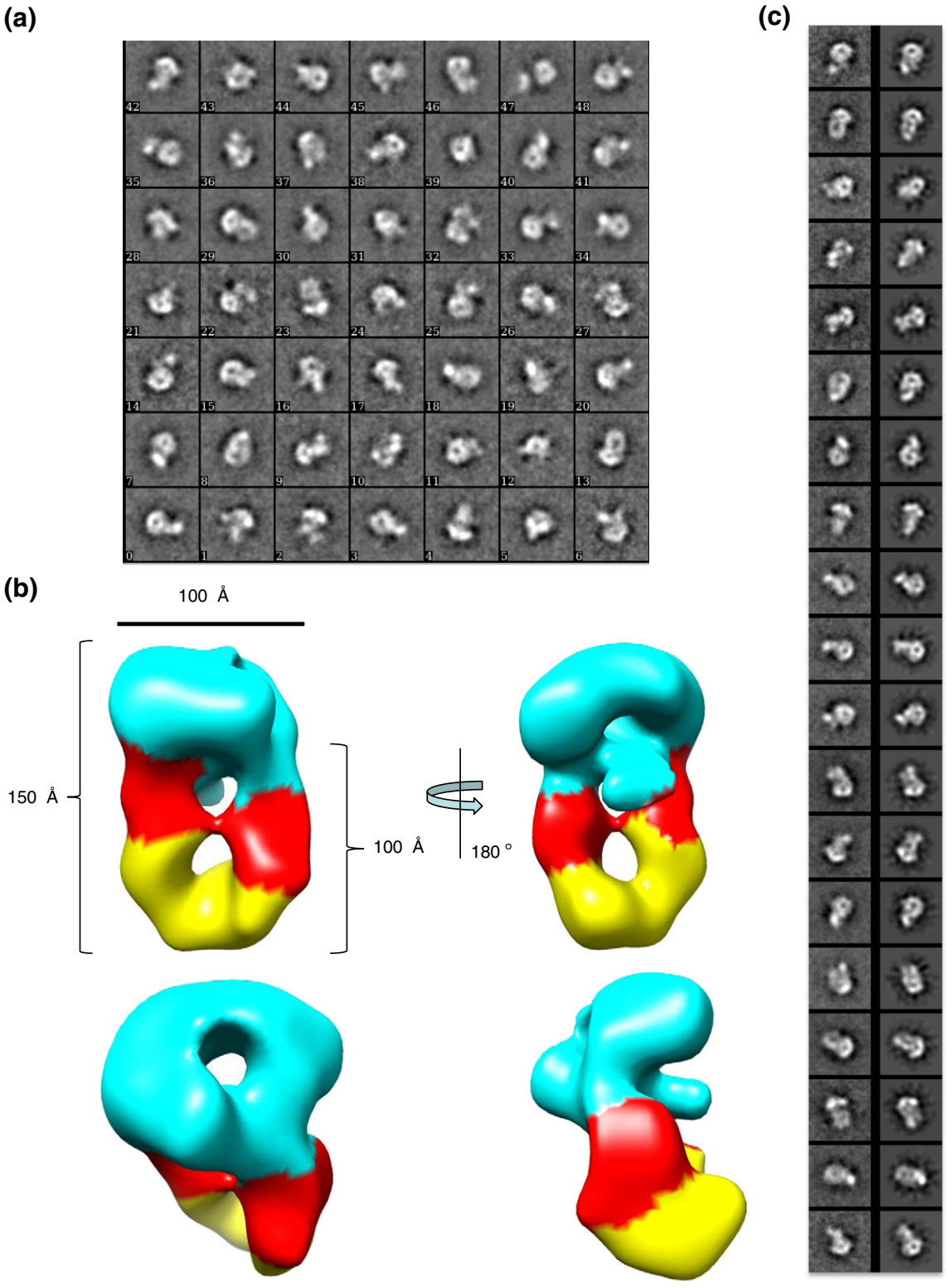

Fig. 5 *(legend on next page)*

similarity between the terminase complex visualized on grid and the model generated by RELION.

A pseudo-atomic model of P22 S-terminase:L-terminase complex

Having established the shape of P22 S-terminase:L-terminase complex (Fig. 5b) and knowing the exact domains involved in assembly (Figs. 3 and 4), we next generated a pseudo-atomic model of the terminase complex. A crystal structure of P22 S-terminase lacking the LBD is available [13]. We then modeled the LBD domain (residues 140–162) based on secondary structure prediction as a helix. Similarly, the L-terminase subunit of bacteriophage P22 was modeled based on the ATPase domain of the close relative Sf6 [23] and the crystal structure of P22 nuclease [25] (Fig. 4b). At first, the X-ray model of nanomeric S-terminase was docked into the hollow density orienting the LBDs toward the new density features corresponding to L-terminase (Fig. 6a). In turn, two L-terminases were fit into the ellipsoid density by positioning the ATPase domain proximal to S-terminase and by slightly rotating the ATPase and nuclease domain with respect to each other. These atomic models were then refined as rigid bodies against the electron microscopy (EM) density using Chimera [50]. In the final pseudo-atomic model, the two L-terminase subunits are not parallel but slightly twisted and contact each other at two distinct points, corresponding to ATPase domains and far C-termini of the nuclease domain (indicated by arrows in Fig. 6a).

Attempts to dock dsDNA inside the pseudo-atomic model of P22 terminase complex suggest two possible modes of binding. DNA could fit through the S-terminase hole (Fig. 6b, model 1) and still interact with both domains of the L-terminase, as previously proposed for the L-terminase of phage Sf6 [23]. Alternatively, DNA could be orthogonal to the S-terminase ring going through the nutcracker (Fig. 6b, model 2), similar to the "inchworm" mechanism proposed by Sun *et al.* for T4 L-terminase [22], which, however, forms pentamers upon binding to procapsid. In both models, the topology of the terminase complex is such that the LBD and L-terminase can simultaneously make contacts with dsDNA.

Discussion

Viral packaging motors are fundamental molecular machines that power the delivery of viral genomes into preformed procapsid shells. Despite growing interest in this field of biology [51], a plethora of individual S-terminase and L-terminase subunit crystal structures [13,16,18,20,22,23,25] and recent advances in single-molecule biophysical analysis of packaging motors [52], not even moderate resolution information exists for a terminase complex. In this study, we purified an *in vivo* assembled complex of P22 terminase subunits and characterized its architecture using biochemical and hybrid structural methods. We found that P22 terminase subunits assemble preferentially into a stable complex containing one nonameric S-terminase bound to two L-terminase subunits (1S-terminase:2L-terminase). While an assembly containing three copies of L-terminase bound to S-terminase (1S-terminase:3L-terminase) was also observed in gas phase, this oligomer was not significantly populated in solution and on grid, suggesting a transient or unstable complex. Unexpectedly, each copy of L-terminase bound to S-terminase associates with only one LBD, suggesting that the entire nonameric S-terminase is not required to bind L-terminase and LBDs helices not participating in L-terminase binding are possibly available to interact with DNA. Only two L-terminase subunits assemble stably onto S-terminase possibly due to steric hindrance between ATPase domains, although we cannot rule out that transient terminase complexes containing more than two copies of L-terminase also form in solution.

What is the functional role of the 1S-terminase:2L-terminase complex in DNA packaging? A satisfactory answer to this question requires further analysis and will be determined by the ability of the terminase complex to bind to and package dsDNA inside empty procapsids. In analogy to phage λ, P22 1S-terminase:2L-terminase complex could represent just a protomer able to further assemble into larger molecular complexes upon binding to DNA or upon docking to portal protein. Similarly, in λ [45,46], the terminase subunits can be isolated as an ~114.2-kDa "protomer", consisting of one L-terminase (gpA) associated with two S-terminase subunits (gpNu1), which is in slow equilibrium with a heterogeneous 13.3S species of ~530 kDa (the "mix"), consisting of four protomers. In the absence of procapsid and viral DNA, polymorphic assemblies of terminase subunits are able to form because of the lack of assembly restraints dictated by other viral proteins and DNA. We observed these aggregates when P22 terminases were co-expressed and purified

Fig. 5. Details of the S-terminase:L-terminase model. (a) ISAC 2D class averages reveal numerous orientations of S-terminase:L-terminase. The class identifier number appears in the lower left for each class average. Approximately 20–40 particles establish each class average. The box size for each class average is 295 Å. (b) Various views of the 3D reconstruction of 2062 particles obtained by RELION. Two molecules of L-terminase (with the ATPase in red and nuclease domain in yellow) are located just below the S-terminase nonamer (cyan). The dimensions of the particle components are shown. (c) ISAC 2D class averages (left) and matching 2D projections of 3D model from RELION (right). Comparisons were generated based using a correlation coefficient with e2classvsproj.py in EMAN2 [68].

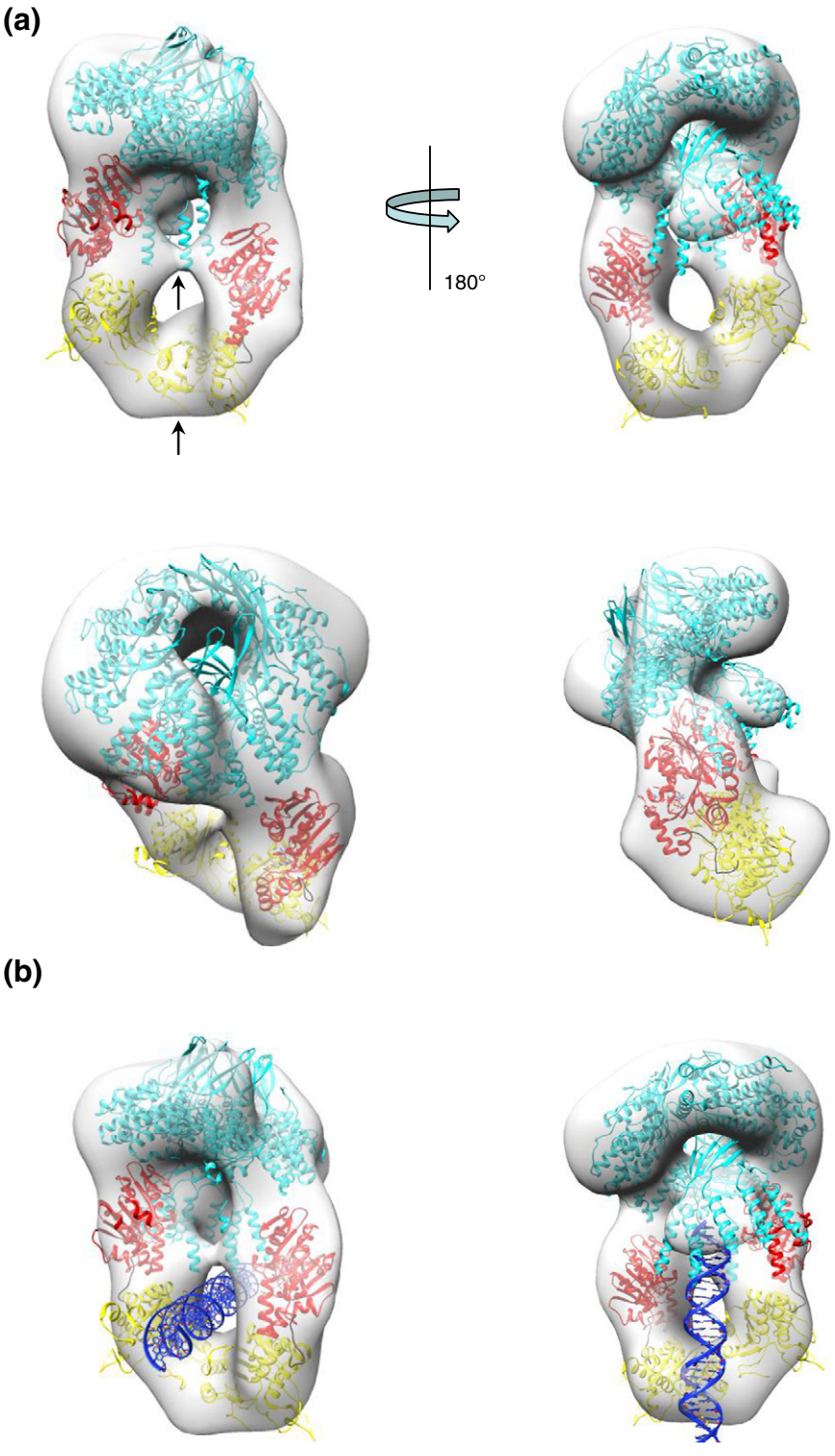

Fig. 6 *(legend on next page)*

in the absence of DDM in lysis buffer, and glycerol and magnesium chloride were not maintained throughout the purification (data not shown). A similar polymorphic distribution of recombinant protein is observed for viral portal proteins that assemble with variable stoichiometry *in vitro* but are always dodecameric in the context of the virion [53–55].

DNA-dependent stimulation of ATPase activity associated to genome packaging

In P22 and other phages, the ATPase activity associated with genome packaging is stimulated by the S-terminase subunit, by a mechanism that remains unknown [5,13]. We previously made the unexpected discovery that the S-terminase-dependent stimulation of ATPase activity in P22 is specifically enhanced by the DNA encoding S-terminase [13], suggesting that the terminase and viral DNA assemble into a functional complex in preparation to docking to procapsid. The stoichiometry of the S-terminase:L-terminase complex elucidated in this paper requires that only two of the nine LBDs of S-terminase contact a pair of L-terminase subunits, leaving "unoccupied" seven LBDs. Because LBD is highly basic and recruits both the L-terminase and *pac* DNA [13], the proposed 9:2 stoichiometry is expected to expose a large number of basic residues at the base of the terminase complex. We propose that P22 S-terminase functions as an "assembly scaffold" to initiate DNA packaging. Using its oligomeric architecture, S-terminase recruits both P22 DNA and L-terminase to form a stable "pre-packaging" complex. In this complex, the S-terminase subunit can simultaneously "recognize" a specific *pac* site in P22 genome and "present" it to the nuclease domain of L-terminase that introduces nicks. The proposed role of S-terminase as an "assembly scaffold" for DNA packaging may help reconcile the different oligomeric state of S-terminase observed in different viruses [13]. Oligomeric rings of different stoichiometry would be sufficient to bring viral DNA and L-terminase in close proximity regardless of the exact number of subunits, possibly explaining why S-terminases have evolved as oligomers of different stoichiometry even in similar viruses such as P22 and Sf6. We postulate that a structural rearrangement must occur in the terminase complex to switch from a pre-packaging conformation (possibly bound to DNA) to an active "packaging" state, where L-terminase is oligomerized at the portal vertex [56]. The latter state has been studied in bacteriophages T4 and T7, where a pentameric stoichiometry of L-terminase was reported (see Refs. [22] and [33]). These studies, however, were carried out in the absence of S-terminase whose actual involvement in DNA packaging remains controversial.

In conclusion, this paper presents the first structural characterization of the terminase complex of bacteriophage P22 and sets up the ground for future higher-resolution structural studies by cryo-EM.

Materials and Methods

Molecular biology techniques

Cloning of the full-length S-terminase (plasmid pMAL-S-terminase) and L-terminase (plasmid pET30b-L-terminase) and L-terminase nuclease domain (residues 289–499) (plasmid pET30b-nuclease) of bacteriophage P22 was previously described [13,14,25]. L-terminase ATPase domain (plasmid pET30b-ATPase) (residues 1–287) was generated by introducing a stop codon at residue 288 of plasmid pET30b-L-terminase. The LBD (residues 140–162 of S-terminase) was amplified by PCR and inserted into a pGEX-6P vector (GE Healthcare Life Sciences) between BamHI and XhoI sites (plasmid pGEX-S-LBD). MBP-LBD was generated by splicing off residues 1–139 from plasmid pMAL-S-terminase. All constructs of L-terminase were also generated by PCR using as template plasmid pET28-L-terminase.

Biochemical techniques

The S-terminase:L-terminase and MBP-LBD:L-terminase complexes were expressed in *Escherichia coli* strain BL21-AI (Life Technologies) by induction at 18 °C for 12–16 h with a final concentration of 0.2% L-arabinose and 0.1 mM IPTG. Cell pellets were dissolved in lysis buffer containing 20 mM Tris–Cl (pH 8.0), 300 mM NaCl, 1 mM $MgCl_2$, 5% glycerol, 0.1% DDM, 3 mM β-mercaptoethanol and 1.0 mM phenylmethylsulfonyl fluoride and cells were disrupted by sonication. Terminase complexes were purified on amylose beads (New England Biolabs), and after washing with 500 ml of lysis buffer, the complexes was incubated with 1 mM AMP-PNP (Sigma) and PreScission Protease to cleave off MBP. On the following day, cleaved species coming off beads were further purified on a Superdex 200 16/60 gel-filtration column (GE Healthcare) in GF buffer [20 mM Tris–Cl (pH 8.0), 150 mM NaCl, 1 mM $MgCl_2$, 5% glycerol and 3 mM β-mercaptoethanol]. The gel-filtration column was calibrated with molecular weight

Fig. 6. Pseudo-atomic model of S-terminase:L-terminase holoenzyme. (a) Various views of the 3D reconstruction in Fig. 5b colored as a transparent gray surface with docked models of one nonameric S-terminase (cyan) and two L-terminase subunits with ATPase and nuclease domains colored red and yellow, respectively. Each L-terminase has an ATPase domain (red) and a nuclease domain (yellow) separated by a short flexible linker (black). Models were rigid body refined into density using the Fitmap function in Chimera [50]. (b) Models of S-terminase:L-terminase binding to dsDNA. In model 1, dsDNA passes through the lower hole between the L-terminase domains. In model 2, the dsDNA is vertically positioned between the two L-terminase domains and abuts the S-terminase C-terminal helices. In this conformation, dsDNA could fit in the S-terminase central channel.

markers as previously described [57]. Isolated S-terminase:L-terminase complex were concentrated to ~10 mg/ml using a 30-MWCO (*m*olecular *w*eight *cut*off) ultrafiltration spin column (Vivaspin 20; Sartorius Stedim Biotech GmbH). Pull-down assays were carried out on glutathione beads (GenScript) as previously described [58,59].

Sedimentation velocity AUC

AUC analysis was carried out in a Beckman XL-A Analytical Ultracentrifuge operating under velocity sedimentation mode available at the Sydney Kimmel Cancer Center X-ray Crystallography and Molecular Interaction Facility. Purified S-terminase:L-terminase and MBP-LBD:L-terminase complexes dissolved at 0.25 mg/ml in 20 mM Tris–Cl (pH 8.0), 150 mM NaCl, 3 mM DTT, 5% glycerol and 1 mM $MgCl_2$ were spun at 35,000 rpm and 40,000 rpm, respectively, at 10 °C. Absorbance values at 280 nm were fit to a continuous sedimentation coefficient [*c*(*s*)] distribution model in SEDFIT [60].

Native MS

Prior to native MS measurement, the purified S-terminase:L-terminase complex was buffer exchanged into 150 mM aqueous ammonium acetate (pH 8.0), by ultrafiltration (Vivaspin 500; Sartorius Stedim Biotech, Germany) with a 10-kDa cutoff. We loaded 1–2 μl of sample, at a final concentration of 2 μM, into a nanoflow gold-plated borosilicate electrospray capillary (made in-house). The higher-order oligomers of S-terminase:L-terminase complex were analyzed on a modified QTOF-2 (Waters/MS Visions) operated on a positive-ion mode. Xenon was used as collision gas. MS parameters were as follows: backing pressure, 10 mbar; capillary, 1300 V; cone, 60 V; extracted cone, 0 V; pressure in the collision cell, 2×10^{-2} mbar; collision energy, 30 V. The sample was analyzed on a modified Exactive Plus EMR Orbitrap instrument (Thermo Fisher Scientific, Bremen) over *m*/*z* range 500–20,000 [61,62]. Manual tuning of the voltage offset on the flatapole, transport multipole, ion lenses was used for mass filtering of the incoming protein ions, as previously described [47]. Nitrogen was used for the HCD cell at a gas pressure of 6–8×10^{-10} bar. MS parameters were as follows: spray voltage, 1.3–1.4 V; source fragmentation, 30 V; source temperature, 250 °C; collision energy, 40–50 V; resolution at *m*/*z* 200, 10,000.

EM specimen preparations

Continuous carbon grids were glow discharged, and 3 μl of sample at a concentration of 0.014 mg/ml was applied to the grid for 1 min. The grid was gently blotted and passed through four 50-μl volumes of 2% uranyl formate. Subsequently, the grid was blotted, air-dried and stored under desiccation.

EM data collection and processing

Images were acquired using a Tecnai 12 electron microscope operating at 120 keV, with a dose near 20 $e^-/Å^2$ and a nominal range of 1.0–2.0 μm underfocus. The continuous carbon grid areas were targeted using Leginon [63] software at a nominal magnification of 52,000× (pixel size of 0.205 nm). Images were recorded using a 4000 × 4000 Tietz F416 CMOS detector (Fig. S1). Approximately 8623 particles were picked from 44 micrographs using Difference of Gaussians Picker [64]. These particles were subjected to reference-free XMIPP Clustering 2D [65], and well-ordered particles were extracted, resulting in 6562 particles. To obtain the best 2D class averages in the presence of any heterogeneity, we produced the sharpest and best-aligned class averages with the ISAC program [66] (Fig. 5a). Using only the S-terminase nonamer low-pass filtered to 60 Å as an initial model (Fig. S2a), we used 3D classification and subsequent gold standard refinement to obtain an asymmetric reconstruction using RELION (Fig. S2). The resolution of the reconstruction was estimated to be approximately 30 Å using the gold standard FSC = 0.143 criterion (Fig. S2b and c) [49]. The 3D EM map has been deposited to the EMDataBank with accession code EMD-6429.

Placement of 3D models in EM density

The crystal structures of S-terminase with modeled extended helices (PDB ID 3P9A) and L-terminase from Sf6 [23] (PDB ID 4IEE) were manually oriented in the EM density based on analysis of 2D class averages and biochemical data shown in Figs. 3 and 4. Subsequently, the models were rigid body refined in the density using the "Fitmap" feature in Chimera (Fig. 6).

Acknowledgements

This work was supported by National Institutes of Health grants R01GM100888 to G.C., R01GM54076 to J.J. and F32GM108310 to R.M. Native MS measurement was performed by Y.Y. and A.J.R.H., who have been supported by the ManiFold project, grant number 317371, and in part by the PRIME-XS project, grant number 262067, both funded by the European Union Seventh Framework Program. Research in this publication includes work carried out at the Sidney Kimmel Cancer Center X-ray Crystallography and Molecular Interaction Facility, which is supported in part by National Cancer Institute grant P30 CA56036. Electron microscopic imaging and reconstruction, performed by R.M., were conducted at the National Resource for Automated Molecular Microscopy that is supported by the National Institutes of Health through a P41 program grant (RR17573) from the National Center for Research Resources.

Appendix A. Supplementary data

Supplementary data to this article can be found online at http://dx.doi.org/10.1016/j.jmb.2015.08.013.

Received 18 May 2015;
Received in revised form 14 August 2015;
Accepted 15 August 2015
Available online 21 August 2015

Keywords:
viral genome-packaging motor;
large terminase;
small terminase bacteriophage P22;
Salmonella virus;
electron microscopy

†R.M. and R.K.L. contributed equally to this work.

Present address: A. Roy, Department of Biochemistry and Molecular Biology, Rutgers University, 683 Hoes Lane, Piscataway, NJ 08854, USA.

Abbreviations used:
S-terminase, small terminase; SBD, S-terminase binding domain; L-terminase, large terminase; LBD, L-terminase binding domain; dsDNA, double-stranded DNA; MBP, maltose binding protein; MS, mass spectrometry; DDM, *n*-dodecyl-β-D-maltoside; AMP-PNP, 5′-adenylyl-β,γ-imidodiphosphate; AUC, analytical ultracentrifugation; EM, electron microscopy; RELION, Regularized Likelihood Optimization; ISAC, Iterative Stable Alignment and Clustering.

References

[1] S. Sun, V.B. Rao, M.G. Rossmann, Genome packaging in viruses, Curr. Opin. Struct. Biol. 20 (2010) 114–120.
[2] S.R. Casjens, The DNA-packaging nanomotor of tailed bacteriophages, Nat. Rev. Microbiol. 9 (2011) 647–657.
[3] A. Bhardwaj, A.S. Olia, G. Cingolani, Architecture of viral genome-delivery molecular machines, Curr. Opin. Struct. Biol. 25 (2014) 1–8.
[4] J.D. Heming, J.B. Huffman, L.M. Jones, F.L. Homa, Isolation and characterization of the herpes simplex virus 1 terminase complex, J. Virol. 88 (2014) 225–236.
[5] V.B. Rao, M. Feiss, The bacteriophage DNA packaging motor, Annu. Rev. Genet. 42 (2008) 647–681.
[6] E.N. Jackson, D.A. Jackson, R.J. Deans, EcoRI analysis of bacteriophage P22 DNA packaging, J. Mol. Biol. 118 (1978) 365–388.
[7] S. Casjens, L. Sampson, S. Randall, K. Eppler, H. Wu, J.B. Petri, et al., Molecular genetic analysis of bacteriophage P22 gene 3 product, a protein involved in the initiation of headful DNA packaging, J. Mol. Biol. 227 (1992) 1086–1099.
[8] R.G. Baumann, L.W. Black, Isolation and characterization of T4 bacteriophage gp17 terminase, a large subunit multimer with enhanced ATPase activity, J. Biol. Chem. 278 (2003) 4618–4627.
[9] G. Leffers, V.B. Rao, Biochemical characterization of an ATPase activity associated with the large packaging subunit gp17 from bacteriophage T4, J. Biol. Chem. 275 (2000) 37127–37136.
[10] D.N. Fuller, D.M. Raymer, V.I. Kottadiel, V.B. Rao, D.E. Smith, Single phage T4 DNA packaging motors exhibit large force generation, high velocity, and dynamic variability, Proc. Natl. Acad. Sci. U. S. A. 104 (2007) 16868–16873.
[11] K. Eppler, E. Wyckoff, J. Goates, R. Parr, S. Casjens, Nucleotide sequence of the bacteriophage P22 genes required for DNA packaging, Virology 183 (1991) 519–538.
[12] C.M. Teschke, K.N. Parent, Let the phage do the work: Using the phage P22 coat protein structures as a framework to understand its folding and assembly mutants, Virology 401 (2010) 119–130.
[13] A. Roy, A. Bhardwaj, P. Datta, G.C. Lander, G. Cingolani, Small terminase couples viral DNA binding to genome-packaging ATPase activity, Structure 20 (2012) 1403–1413.
[14] A. Roy, A. Bhardwaj, G. Cingolani, Crystallization of the nonameric small terminase subunit of bacteriophage P22, Acta Crystallogr. Sect. F: Struct. Biol. Cryst. Commun. F67 (2011) 104–110.
[15] D. Nemecek, E.B. Gilcrease, S. Kang, P.E. Prevelige Jr., S. Casjens, G.J. Thomas Jr., Subunit conformations and assembly states of a DNA-translocating motor: The terminase of bacteriophage P22, J. Mol. Biol. 374 (2007) 817–836.
[16] C.R. Buttner, M. Chechik, M. Ortiz-Lombardia, C. Smits, I.O. Ebong, V. Chechik, et al., Structural basis for DNA recognition and loading into a viral packaging motor, Proc. Natl. Acad. Sci. U. S. A. 109 (2012) 811–816.
[17] H. Zhao, C.J. Finch, R.D. Sequeira, B.A. Johnson, J.E. Johnson, S.R. Casjens, et al., Crystal structure of the DNA-recognition component of the bacterial virus Sf6 genome-packaging machine, Proc. Natl. Acad. Sci. U. S. A. 107 (2010) 1971–1976.
[18] S. Sun, S. Gao, K. Kondabagil, Y. Xiang, M.G. Rossmann, V.B. Rao, Structure and function of the small terminase component of the DNA packaging machine in T4-like bacteriophages, Proc. Natl. Acad. Sci. U. S. A. 109 (2012) 817–822.
[19] T. de Beer, J. Fang, M. Ortega, Q. Yang, L. Maes, C. Duffy, et al., Insights into specific DNA recognition during the assembly of a viral genome packaging machine, Mol. Cell 9 (2002) 981–991.
[20] H. Zhao, Y.N. Kamau, T.E. Christensen, L. Tang, Structural and functional studies of the phage Sf6 terminase small subunit reveal a DNA-spooling device facilitated by structural plasticity, J. Mol. Biol. 423 (2012) 413–426.
[21] S.R. Casjens, P.A. Thuman-Commike, Evolution of mosaically related tailed bacteriophage genomes seen through the lens of phage P22 virion assembly, Virology 411 (2011) 393–415.
[22] S. Sun, K. Kondabagil, B. Draper, T.I. Alam, V.D. Bowman, Z. Zhang, et al., The structure of the phage T4 DNA packaging motor suggests a mechanism dependent on electrostatic forces, Cell 135 (2008) 1251–1262.
[23] H. Zhao, T.E. Christensen, Y.N. Kamau, L. Tang, Structures of the phage Sf6 large terminase provide new insights into DNA translocation and cleavage, Proc. Natl. Acad. Sci. U. S. A. 110 (2013) 8075–8080.
[24] C. Smits, M. Chechik, O.V. Kovalevskiy, M.B. Shevtsov, A.W. Foster, J.C. Alonso, et al., Structural basis for the nuclease activity of a bacteriophage large terminase, EMBO Rep. 10 (2009) 592–598.
[25] A. Roy, G. Cingolani, Structure of p22 headful packaging nuclease, J. Biol. Chem. 287 (2012) 28196–28205.
[26] M. Nadal, P.J. Mas, A.G. Blanco, C. Arnan, M. Sola, D.J. Hart, et al., Structure and inhibition of herpesvirus DNA packaging terminase nuclease domain, Proc. Natl. Acad. Sci. U. S. A. 107 (2010) 16078–16083.
[27] S. Selvarajan Sigamani, H. Zhao, Y.N. Kamau, J.D. Baines, L. Tang, The structure of the herpes simplex virus DNA-

packaging terminase pUL15 nuclease domain suggests an evolutionary lineage among eukaryotic and prokaryotic viruses, J. Virol. 87 (2013) 7140–7148.
[28] S. Casjens, P.R. Weigele (Eds.), Viral Genome Packaging Machines: Genetics, Structure, and Mechanism, Kluwer Academic/Plenum Publishers and Landes Bioscience/Eurekah.com, Georgetown, TX and New York, NY, 2005.
[29] C.E. Catalano, Viral Genome Packaging Machines: Genetics, Structure, and Mechanism. , Kluwer Academic/Plenum Publishers and Landes Bioscience/Eurekah.com, Georgetown, TX and New York, NY, 2005.
[30] A.R. Poteete, D. Botstein, Purification and properties of proteins essential to DNA encapsulation by phage P22, Virology 95 (1979) 565–573.
[31] H. Wu, L. Sampson, R. Parr, S. Casjens, The DNA site utilized by bacteriophage P22 for initiation of DNA packaging, Mol. Microbiol. 45 (2002) 1631–1646.
[32] D. Botstein, M. Levine, Intermediates in the synthesis of phage P22 DNA, Cold Spring Harbor Symp. Quant. Biol. 33 (1968) 659–667.
[33] M.I. Dauden, J. Martin-Benito, J.C. Sanchez-Ferrero, M. Pulido-Cid, J.M. Valpuesta, J.L. Carrascosa, Large terminase conformational change induced by connector binding in bacteriophage T7, J. Biol. Chem. 288 (2013) 16998–17007.
[34] S.R. Casjens, E.B. Gilcrease, Determining DNA packaging strategy by analysis of the termini of the chromosomes in tailed-bacteriophage virions, Methods Mol. Biol. 502 (2009) 91–111.
[35] A.S. Olia, J. Al-Bassam, D.A. Winn-Stapley, L. Joss, S.R. Casjens, G. Cingolani, Binding-induced stabilization and assembly of the phage P22 tail accessory factor gp4, J. Mol. Biol. 363 (2006) 558–576.
[36] K. Lorenzen, A.S. Olia, C. Uetrecht, G. Cingolani, A.J. Heck, Determination of stoichiometry and conformational changes in the first step of the P22 tail assembly, J. Mol. Biol. 379 (2008) 385–396.
[37] A.S. Olia, P.E. Prevelige Jr., J.E. Johnson, G. Cingolani, Three-dimensional structure of a viral genome-delivery portal vertex, Nat. Struct. Mol. Biol. 18 (2011) 597–603.
[38] H. Zheng, A.S. Olia, M. Gonen, S. Andrews, G. Cingolani, T. Gonen, A conformational switch in bacteriophage p22 portal protein primes genome injection, Mol. Cell 29 (2008) 376–383.
[39] J. Tang, G.C. Lander, A. Olia, R. Li, S. Casjens, P. Prevelige Jr., et al., Peering down the barrel of a bacteriophage portal: The genome packaging and release valve in p22, Structure 19 (2011) 496–502.
[40] A.S. Olia, A. Bhardwaj, L. Joss, S. Casjens, G. Cingolani, Role of gene 10 protein in the hierarchical assembly of the bacteriophage P22 portal vertex structure, Biochemistry 46 (2007) 8776–8784.
[41] A. Bhardwaj, A.S. Olia, N. Walker-Kopp, G. Cingolani, Domain organization and polarity of tail needle GP26 in the portal vertex structure of bacteriophage P22, J. Mol. Biol. 371 (2007) 374–387.
[42] A.S. Olia, S. Casjens, G. Cingolani, Structural plasticity of the phage P22 tail needle gp26 probed with xenon gas, Protein Sci. 18 (2009) 537–548.
[43] J. King, E.V. Lenk, D. Botstein, Mechanism of head assembly and DNA encapsulation in *Salmonella* phage P22. II. Morphogenetic pathway, J. Mol. Biol. 80 (1973) 697–731.
[44] J. Ebel-Tsipis, D. Botstein, M.S. Fox, Generalized transduction by phage P22 in *Salmonella typhimurium*. I. Molecular origin of transducing DNA, J. Mol. Biol. 71 (1972) 433–448.
[45] N.K. Maluf, Q. Yang, C.E. Catalano, Self-association properties of the bacteriophage lambda terminase holoenzyme: Implications for the DNA packaging motor, J. Mol. Biol. 347 (2005) 523–542.
[46] N.K. Maluf, H. Gaussier, E. Bogner, M. Feiss, C.E. Catalano, Assembly of bacteriophage lambda terminase into a viral DNA maturation and packaging machine, Biochemistry 45 (2006) 15259–15268.
[47] J. Snijder, M. van de Waterbeemd, E. Damoc, E. Denisov, D. Grinfeld, A. Bennett, et al., Defining the stoichiometry and cargo load of viral and bacterial nanoparticles by Orbitrap mass spectrometry, J. Am. Chem. Soc. 136 (2014) 7295–7299.
[48] J.C. Leavitt, E.B. Gilcrease, K. Wilson, S.R. Casjens, Function and horizontal transfer of the small terminase subunit of the tailed bacteriophage Sf6 DNA packaging nanomotor, Virology 440 (2013) 117–133.
[49] S.H. Scheres, RELION: Implementation of a Bayesian approach to cryo-EM structure determination, J. Struct. Biol. 180 (2012) 519–530.
[50] E.F. Pettersen, T.D. Goddard, C.C. Huang, G.S. Couch, D.M. Greenblatt, E.C. Meng, et al., UCSF Chimera—A visualization system for exploratory research and analysis, J. Comput. Chem. 25 (2004) 1605–1612.
[51] P. Guo, Z. Zhao, J. Haak, S. Wang, D. Wu, B. Meng, et al., Common mechanisms of DNA translocation motors in bacteria and viruses using one-way revolution mechanism without rotation, Biotechnol. Adv. 32 (2014) 853–872.
[52] S. Liu, G. Chistol, C.L. Hetherington, S. Tafoya, K. Aathavan, J. Schnitzbauer, et al., A viral packaging motor varies its DNA rotation and step size to preserve subunit coordination as the capsid fills, Cell 157 (2014) 702–713.
[53] G. Cingolani, S.D. Moore, P.E. Prevelige Jr., J.E. Johnson, Preliminary crystallographic analysis of the bacteriophage P22 portal protein, J. Struct. Biol. 139 (2002) 46–54.
[54] G.C. Lander, L. Tang, S.R. Casjens, E.B. Gilcrease, P. Prevelige, A. Poliakov, et al., The structure of an infectious p22 virion shows the signal for headful DNA packaging, Science 312 (2006) 1791–1795.
[55] B.L. Trus, N. Cheng, W.W. Newcomb, F.L. Homa, J.C. Brown, A.C. Steven, Structure and polymorphism of the UL6 portal protein of herpes simplex virus type 1, J. Virol. 78 (2004) 12668–12671.
[56] B.T. Andrews, C.E. Catalano, Strong subunit coordination drives a powerful viral DNA packaging motor, Proc. Natl. Acad. Sci. U. S. A. 110 (2013) 5909–5914.
[57] R.K. Lokareddy, A. Bhardwaj, G. Cingolani, Atomic structure of dual-specificity phosphatase 26, a novel p53 phosphatase, Biochemistry 52 (2013) 938–948.
[58] G. Mitrousis, A.S. Olia, N. Walker-Kopp, G. Cingolani, Molecular basis for the recognition of snurportin 1 by importin beta, J. Biol. Chem. 283 (2008) 7877–7884.
[59] K. Lott, A. Bhardwaj, G. Mitrousis, N. Pante, G. Cingolani, The importin beta binding domain modulates the avidity of importin beta for the nuclear pore complex, J. Biol. Chem. 285 (2010) 13769–13780.
[60] P. Schuck, Size-distribution analysis of macromolecules by sedimentation velocity ultracentrifugation and lamm equation modeling, Biophys. J. 78 (2000) 1606–1619.
[61] R.J. Rose, E. Damoc, E. Denisov, A. Makarov, A.J. Heck, High-sensitivity Orbitrap mass analysis of intact macromolecular assemblies, Nat. Methods 9 (2012) 1084–1086.
[62] S. Rosati, R.J. Rose, N.J. Thompson, E. van Duijn, E. Damoc, E. Denisov, et al., Exploring an orbitrap analyzer for the characterization of intact antibodies by native mass spectrometry, Angew. Chem. 51 (2012) 12992–12996.

[63] C. Suloway, J. Pulokas, D. Fellmann, A. Cheng, F. Guerra, J. Quispe, et al., Automated molecular microscopy: The new Leginon system, J. Struct. Biol. 151 (2005) 41–60.
[64] N.R. Voss, C.K. Yoshioka, M. Radermacher, C.S. Potter, B. Carragher, DoG Picker and TiltPicker: Software tools to facilitate particle selection in single particle electron microscopy, J. Struct. Biol. 166 (2009) 205–213.
[65] C.O. Sorzano, J.R. Bilbao-Castro, Y. Shkolnisky, M. Alcorlo, R. Melero, G. Caffarena-Fernandez, et al., A clustering approach to multireference alignment of single-particle projections in electron microscopy, J. Struct. Biol. 171 (2010) 197–206.
[66] Z. Yang, J. Fang, J. Chittuluru, F.J. Asturias, P.A. Penczek, Iterative stable alignment and clustering of 2D transmission electron microscope images, Structure 20 (2012) 237–247.
[67] J. Yang, R. Yan, A. Roy, D. Xu, J. Poisson, Y. Zhang, The I-TASSER Suite: Protein structure and function prediction, Nat. Methods 12 (2015) 7–8.
[68] G. Tang, L. Peng, P.R. Baldwin, D.S. Mann, W. Jiang, I. Rees, et al., EMAN2: An extensible image processing suite for electron microscopy, J. Struct. Biol. 157 (2007) 38–46.